

RPN109

Air Force Report No.
SAMSO-TR-69-304

Aerospace Report No.
TR-0066(5220-50)-4
(Formerly TR-0200(4220-50)-4)

SPACE, TIME, AND ENERGY DISTRIBUTIONS OF NEUTRONS
AND X RAYS FROM A FOCUSED PLASMA DISCHARGE

Prepared by

M. J. Bernstein, D. A. Meskan, and H. L. L. van Paassen
Plasma Research Laboratory

69 SEP 04

Laboratory Operations
AEROSPACE CORPORATION

Prepared for

SPACE AND MISSILE SYSTEMS ORGANIZATION
AIR FORCE SYSTEMS COMMAND
LOS ANGELES AIR FORCE STATION
Los Angeles, California

This document has been approved for public release
and sale; its distribution is unlimited.

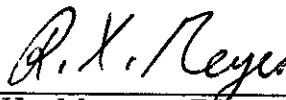
FOREWORD

This report is published by The Aerospace Corporation, El Segundo, California, under Air Force Contract No. F04701-69-C-0066.

This report, which documents research carried out from July 1967 to February 1969, was submitted on 11 August 1969 to Lieutenant Edward M. Williams, Jr., SMTAE, for review and approval.

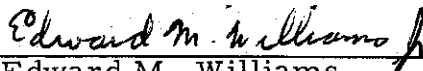
The authors acknowledge the many stimulating discussions with G. G. Comisar and M. H. Dazey and thank the former for calculating the flux ratios. We are indebted to R. S. White for his advice and assistance in preparing and analyzing the nuclear emulsions. The technical support of G. Jameson, R. A. Shenk, R. L. Walter, and E. Winet was greatly appreciated. D. A. Meskan is now with Physics International, San Leandro, California.

Approved



R. X. Meyer, Director
Plasma Research Laboratory

Publication of this report does not constitute Air Force approval of the report's findings or conclusions. It is published only for the exchange and stimulation of ideas.



Edward M. Williams
2nd Lt., United States Air Force
Project Officer

ABSTRACT

The energy spectrum and spatial distribution of neutrons emitted by a plasma focus device were measured with nuclear emulsions and scintillation detectors, and the results are reported. The average energy of the D-D neutrons emitted along the axis was shifted ~ 500 keV, corresponding to an axial center-of-mass velocity of 2×10^8 cm/sec for the reacting deuterons. A 11% anisotropy in the neutron fluxes measured in the forward and radial directions correlates with an axially streaming plasma which is not isotropic; the reacting deuterons collide predominantly in the radial direction. Time-resolved collimation measurements of the emitted neutrons showed an axial translation of the neutron source corresponding to velocities up to 2×10^8 cm/sec; this correlates with the nonsimultaneous pinching of the noncylindrical plasma along the axis. Plasma densities of $\sim 2 \times 10^{20}$ cm⁻³ and ion temperatures of 2 keV were consistent with observed neutron yields of 10^{10} and pulse widths of 60 nsec. X-ray intensity measurements were made for x-ray energies of $7 < E_p < 30$ keV and showed an E_p^{-2} dependence which does not agree with plasma Bremsstrahlung, but appears to result from anode bombardment of axially-accelerated electrons with energies > 200 keV. The line radiation corresponded to that of fairly cold ions.

CONTENTS

FOREWORD	ii
ABSTRACT	iii
I. INTRODUCTION	1
II. APPARATUS	3
III. DISCHARGE BEHAVIOR	5
IV. NEUTRON MEASUREMENTS	7
A. Nuclear Emulsion Measurements of Neutron Energy Spectra	7
B. Flux and Time-of-Flight Measurements	8
C. Spatial and Temporal Resolution of the Neutron Source	12
V. ANALYSIS OF NEUTRON MEASUREMENTS	17
VI. X-RAY MEASUREMENTS	21
A. Experiment	21
B. Interpretation of X-Ray Results	24
VII. CONCLUSIONS	27
REFERENCES AND FOOTNOTES	29

FIGURES

1.	Schematic Diagram of Apparatus	4
2.	Framing and Streak Photographs of Radial Collapse Using TRW Image-Converter Camera	6
3.	Oscilloscope Traces of dI/dt and the Current I	6
4.	Energy Spectra From Nuclear Emulsions	9
5.	Neutron Flux Ratio Measurements	10
6.	Neutron Collimation Measurements	13
7.	Axial Distribution of Neutron Intensity	14
8.	Time History of Neutron Source as a Function of Axial Position	18
9.	X-Ray Spectra With Ross Filters	22
10.	Side-on X-Ray Pinhole Photograph Through 0.05-mm-thick Be Window	23

TABLES

1.	Neutron Flux Ratios Parallel and Perpendicular to the Discharge Axis (0° and 90°)	11
----	--	----

I. INTRODUCTION

Different mechanisms have been proposed to explain the intense production of neutrons and x rays generated by the dense deuterium plasmas formed in plasma focus devices, for which neutron yields of 10^9 to 10^{10} , pulse widths of ~ 100 nsec, and plasma densities of 2×10^{19} to 3×10^{20} cm^{-3} have been reported.¹⁻⁴ We present the results of measuring the energy spectrum of axially-emitted neutrons, the neutron-flux anisotropy, and the time-resolved spatial distribution of the neutron source. These results show that both the axial jetting and the location of the neutron-producing plasma correlate with the nonsimultaneous compression of the noncylindrical pinch. The measured center-of-mass velocity of the reacting deuterons is significantly larger than previously reported elsewhere.

Results of flux-isotropy measurements on a dense plasma focus and the lack of target effects led to the assumption of a quasi-stationary thermonuclear plasma.⁵ Other measurements of both flux isotropy and anisotropic shifts in the neutron energies led to the "moving-boiler" model of neutron production,⁶ in which the reacting deuterons are isotropic in their center of mass (c. o. m.), but the plasma has an axial velocity up to 10^8 cm/sec. Nuclear-emulsion measurements⁴ made using a focused pinch in a paraboloidal geometry showed a shift of at least 400 keV in the average energy of the axially emitted neutrons, which corresponds to a c. o. m. velocity of 1.6×10^8 cm/sec. Recent measurements of the integrated neutron flux and energy measurements of the early neutrons gave results⁷ which agreed with a model of a moving thermal plasma having an axial velocity averaging 1.2×10^8 cm/sec.

It is paradoxical that a plasma velocity greater than 10^8 cm/sec with a neutron production time of 100 nsec implies that a dense plasma blob moves more than 10 cm during the neutron production, whereas the visible length of the plasma is only 2 to 4 cm. Therefore, it has been suggested that only the early part of the neutron production is characterized by a high-velocity streaming.⁷

Determinations of electron temperatures in very hot plasmas are usually dependent on assuming plasma Bremsstrahlung and measuring the attenuation of the emitted x rays with various thicknesses of absorbing material.⁸ By these means, electron temperatures of a few keV were derived for focused z-pinchs.^{1, 2} Unfortunately, x-ray spectra very different from that of a thermal continuum also have almost the same attenuation through absorbers. The use of different filters resulted in inferred electron temperatures as high as 8 keV when a thermal plasma with copper contamination was assumed.³ Earlier measurements of the x-ray spectra using an all-copper anode resulted in a power-law spectrum that is inconsistent with radiation from a thermal plasma.⁴

In this paper, we describe briefly the experimental apparatus and operation of the device. Then we discuss measurements of the neutron energy spectrum made with nuclear emulsions, neutron-flux measurements with scintillation detectors, and neutron collimation measurements, followed by an analysis of the results. Last, we describe measurements of the x-ray spectrum made with Ross filters and discuss the results.

II. APPARATUS

The coaxial discharge device is similar to that first used by Mather in producing a dense plasma focus.² The apparatus is shown schematically in Fig. 1. Two coaxial copper cylinders formed the electrodes. The anode diameter was 7.8 cm, and the perforated outer cathode had an inner diameter of 15.0 cm. The coaxial pyrex insulator extended 5 cm along the anode, which ranged in length from 21 to 23 cm. Normally, the hollow anode had an insert of tungsten in the copper end to retard erosion. (A discussion of effects of anode material on the neutron production from the focused pinch in a paraboloidal geometry will be presented in a future paper.) Numerous ports for visual and x-ray viewing of the plasma were located on the aluminum vacuum chamber, which had an inner diameter of 27 cm. The gas pressure was measured with an oil manometer.

The capacitor bank consisted of twelve 14- μ F condensers connected with low-inductance feed plates to the central header. For the early part of the work reported here, the capacitors were switched with six GE 7703 ignitrons. In this case, initial bank voltage was 14 kV, which produced a peak current of 600 kA using a deuterium filling of 3 Torr. Later the capacitor bank was modified and switched with four low-pressure spark gaps similar to those originally described.⁹ Operations with these gaps was with a bank voltage of 18 kV, giving a peak current of 820 kA with 5 Torr deuterium in the chamber. The total external inductance of the circuit using spark gaps was 13 nH.

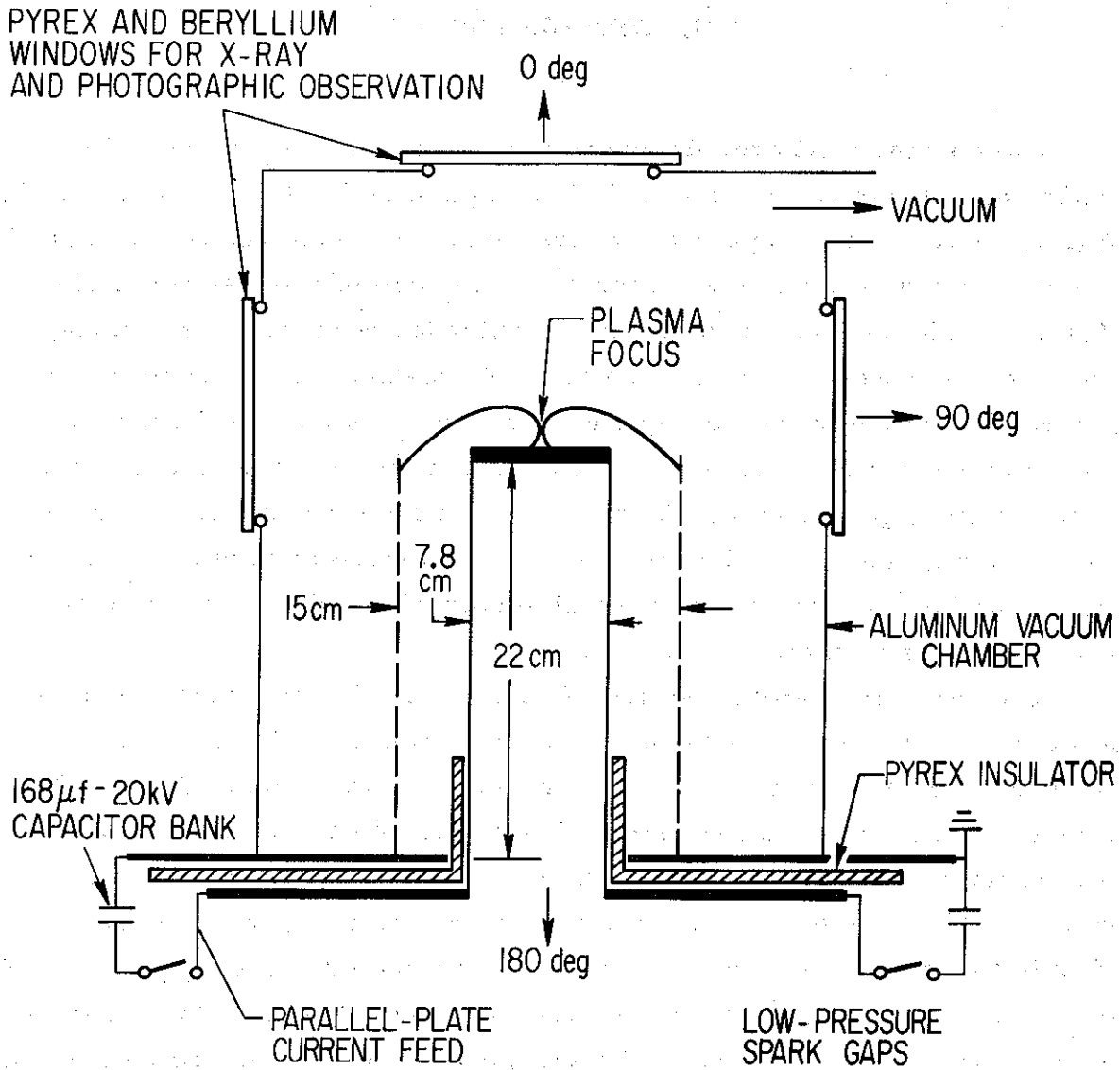


Figure 1. Schematic Diagram of Apparatus

III. DISCHARGE BEHAVIOR

The acceleration phase of the coaxial discharge leading to the z-pinch at the end of the electrodes has been well investigated.^{2, 10} After an initial breakdown, the neutral gas is snowplowed by the $j \times B$ driven current sheet. Since the magnetic field decreases with radius, the plasma is driven both axially and radially outward, while perforations in the cathode keep the plasma from piling up on the inside of the electrode. When the discharge reaches the end of the anode, the snowplowed plasma acts as an inertial cap, while the stored magnetic-field energy produces a rapid radial pinch across the end of the anode. A set of framing pictures and a streak picture taken during the collapse are shown in Fig. 2.

The fast pinching of the plasma increases the discharge inductance L with a corresponding drop of 20 to 40% in the discharge current. The product LI is assumed to remain about constant during the collapse since initial parameters are chosen so that the collapse occurs at about peak current. Traces of I and dI/dt are shown in Fig. 3. The large values of $I dL/dt$ produced by the pinch can generate electric fields up to 400 kV/cm, and intense pulses of very hard x rays are often detected. Neutron yields of 5×10^9 to 2×10^{10} per discharge were obtained with a bank voltage of 18 kV (27 kJ), while operation at 14 kV (17 kJ) gave yields up to 3×10^9 per discharge.

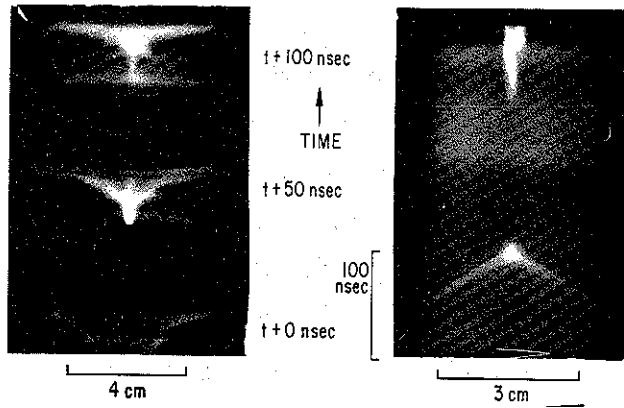


Figure 2. Framing and Streak Photographs of Radial Collapse Using TRW Image-Converter Camera
(Framing exposure 5 nsec; streak slit 0.8 cm above anode)

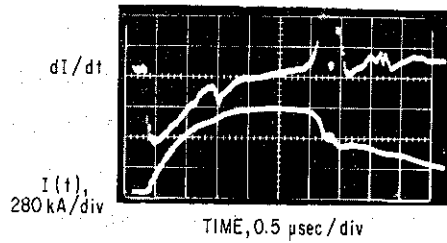


Figure 3. Oscilloscope Traces of dI/dt and the Current I
(Operating conditions 18 kV with 5-Torr deuterium)

IV. NEUTRON MEASUREMENTS

A. NUCLEAR EMULSION MEASUREMENTS OF NEUTRON ENERGY SPECTRA

Ilford K-2 200- μ -thick nuclear emulsions placed on the axis at 0 and 180 deg approximately 28 cm from the anode tip were exposed to a total of 2.8×10^{11} neutrons during 169 discharges. Each emulsion was surrounded by a lead x-ray shield, 0.65 cm thick. Standard procedures for photographically developing and microscopically scanning the emulsions were used to obtain recoil proton ranges.¹¹⁻¹³ Through use of the range-energy relationship for the emulsion, raw data consisting of a distribution of recoil proton energies $f_p(E)$ were generated.

Mass associated with the experimental apparatus and the lead x-ray shield caused neutron scattering, which was a source of error when converting the recoil proton spectra to the neutron energy spectra $f_n(E)$.

Laboratory frame energies of a recoil proton and incident neutron are related by $E_p = E_n \cos^2 \phi$, where ϕ is the laboratory angle between the initial neutron and resultant proton velocities. A neutron which has been scattered by high-z material prior to collision with the proton can have almost all of its initial energy, and there is a possibility for error in analysis because of the uncertainty in ϕ . It is important to note that E_p found from the measured length of a recoil proton track represents the minimum possible energy of the incident neutron; i. e., errors in estimating ϕ lead to errors in E_n , but $E_n(\text{true}) \geq E_p$.

Assuming the neutron energy anisotropy to be of the form $E_n = 2.45 + \Delta E_n \cos \theta$ MeV allows one to estimate the minimum recoil proton energy expected for the emulsion at $\theta = 0$ deg. If data corresponding to $\phi > \phi_c$ are rejected during scanning of the emulsion, the minimum recoil proton energy is given by $E_p(\text{min}) = 2.45 \cos^2 \phi_c$ MeV; e. g., $\phi_c = 30$ deg identifies recoil protons having $E_p < 1.84$ MeV with scattered neutrons.

A similar procedure can be followed for the 180-deg emulsion except that one rejects proton tracks that lead to $E_n > 2.5$ MeV. Rejection of these tracks is justified only if the assumed form of energy anisotropy is correct for $\theta = 180$ deg. Confidence in the assumption is increased when the neutron energy spectrum from the 0-deg emulsion is shifted toward energies greater than 2.5 MeV, as it is from our measurements. Nonetheless, the energy spectra from the 180-deg emulsion remain more ambiguous with regard to scattered neutron content than do the 0-deg spectra.

The error due to scattered neutrons can be reduced by making ϕ_c very small. Alternatively, data obtained for large ϕ_c can be analyzed numerically by studying the effect on the resulting spectra of reducing ϕ_c . The latter approach has the benefit of requiring less emulsion scanning and was considered sufficient for this experiment.

Recoil proton energy spectra corrected for scattering according to this procedure and the derived neutron energy spectra are shown in Fig. 4.

The neutron spectra indicate an average energy shift from 2.45 MeV of $E_n \sim 550$ keV and a maximum shift $\Delta E_n(\text{max}) \sim 750$ keV. All the spectra suggest that the neutron energy shift was in the range $300 \leq \Delta E_n \leq 750$ keV for the 169 discharges included in the data. The energy shift maximum is confirmed by the recoil proton energy spectrum taken at 0 deg, which extends to $E_p \sim 3.3$ MeV. A significant shortage of neutrons with $E_n \sim 2.45$ MeV is also evident.

B. FLUX AND TIME-OF-FLIGHT MEASUREMENTS

Time-resolved ratios of the neutron fluxes emitted at 0 deg and 90 deg were determined from measurements using a pair of scintillation detectors. Photomultipliers of type RCA 6810A were used with appropriate circuits to give linear outputs of up to 10 V across a 50- Ω load, and the signals were displayed on a 100-MHz Fairchild 777 dual-beam oscilloscope. A pair of typical scope traces is shown in Fig. 5. (The combined rise time of NE102 scintillation plastic, photomultiplier, and oscilloscope was about 4 nsec.)

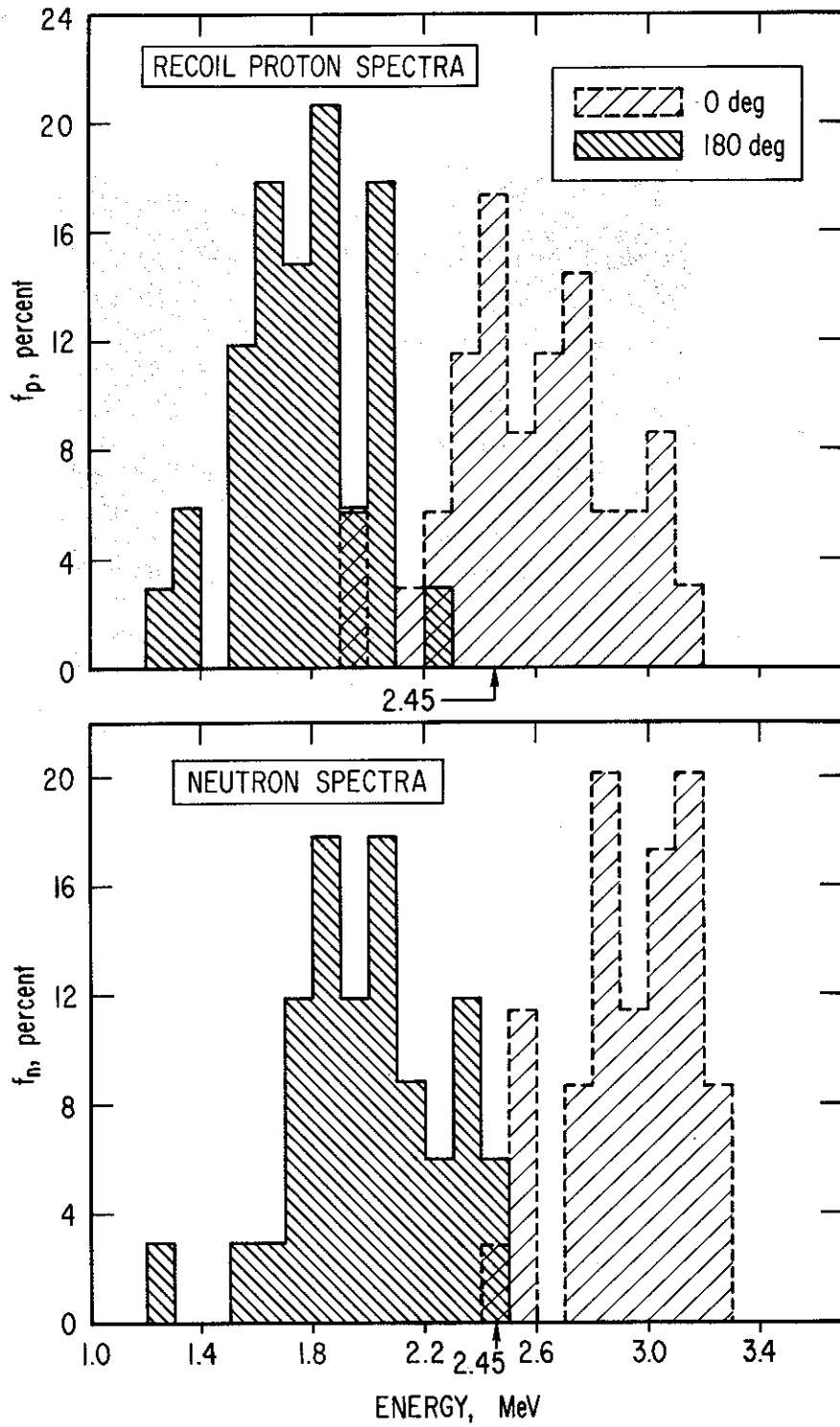
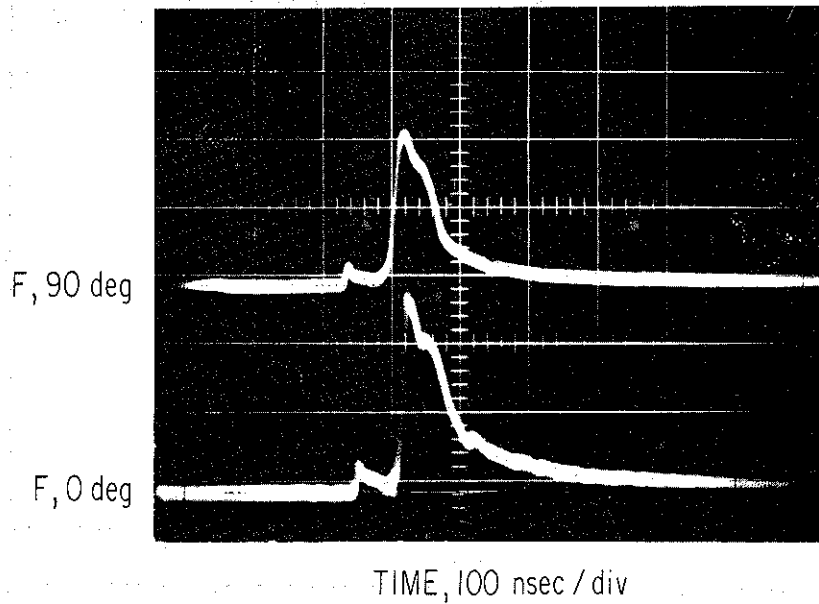


Figure 4. Energy Spectra From Nuclear Emulsions



**Figure 5. Neutron Flux Ratio Measurements
(Detectors balanced at 90 deg)**

The detectors were located 180 cm from the neutron source, and paraffin collimators were used to reduce the intensity of neutrons scattered by the vacuum chamber. Other scattered neutrons were differentiated by time-of-flight delays. Attenuation of the neutron flux passing through the vacuum chamber was the same for measurements at both 90 deg and 0 deg. The flux ratios were measured from the intensity peaks of the neutron pulses, with the detectors adjusted to give equal outputs at 90 deg.¹⁴ An average value for the signal ratio of $1.28 \pm .04$ was obtained although variations in the flux ratio during the pulse were occasionally observed.

The relative light output from the scintillator as a function of average neutron energy was computed, taking into account the nonlinear dependence of light output on recoil-proton energy^{15, 16} and the energy dependence of the n-p cross section.¹⁷ Table 1 gives corrected values of the measured neutron flux ratio $F(0)/F(90)$ for different values of the energy shift ΔE_n , where $\Delta E_n = E_n(0) - E_n(90)$ is the difference between the average energy of neutrons emitted at 0 deg and those emitted at 90 deg; $E_n(90)$ is assumed to be about 2.5 MeV, but is not critical for the calculations (time-of-flight measurements gave values of $E_n(90)$ ranging from 2.45 to 2.60 MeV).

Table 1. Neutron Flux Ratios Parallel and Perpendicular to the Discharge Axis (0° and 90°)

ΔE_n^a	Adjusted Measurements ^b	3-Dimen Isotropic ^c	2-Dimen Radial (2 keV) ^d
0 keV	1.28	1.00	0.82
200	1.21	1.08	0.88
400	1.14	1.17	0.96
600	1.06	1.26	1.04

^a Difference in average neutron energies at 0° and 90° .

^b Measured signal ratio of $1.28 \pm .04$ corrected for scintillator response to different average neutron energies at 0° and 90° .

^{c, d} Calculated flux ratios for 3-dimensional and 2-dimensional plasmas having axial velocities which give ΔE_n .

Measurements of ΔE_n were obtained by time-of-flight differences of the neutron pulses in the flux measurements. Values of the energy shifts measured from the leading edges of the neutron pulses varied from 100 to 300 keV, whereas the energy shifts determined from the sharp peaks of the pulses ranged from 300 to 600 keV. Errors were ± 100 keV.

C. SPATIAL AND TEMPORAL RESOLUTION OF THE NEUTRON SOURCE

The intensity distribution of the neutron source along the axis was measured using a pair of scintillation detectors located 400 cm from the axis in the radial direction. The detectors (similar to those used for the flux measurements) were used to observe both the total neutron pulse and an axially-resolved neutron pulse through a collimator. Primary collimation of the neutrons to one detector was accomplished with blocks of polyethylene forming a collimating slot 0.3 cm high (in the axial direction) by 30 cm long. Since luminous-light and x-ray photography showed that the plasma radius was less than 1 mm, ^{1,2} radial collimation was not attempted and the slot width was 2 to 4 cm. The collimator began 18 cm from the discharge axis and was moved in the axial direction. Additional blocks of polyethylene and paraffin were used to reduce the signal due to scattered neutrons. Details of the collimator will be described in a future paper. The detector monitoring the total neutron pulse also used large-aperture collimation to reduce the signal due to scattered neutrons. Typical traces of the neutron pulses are shown in Fig. 6. For most of the slots, especially those with the highest neutron yields, the pulse had a single peak. However, there was no correlation between the shape of the pulse and the neutron yield. The pulse widths (FWHM) ranged from 45 to 65 nsec for the total pulse and from 25 to 45 nsec for the collimated pulse. Rise times of the pulses were around 20 to 25 nsec and varied little with axial position. We determined axial distributions of the neutron source by normalizing the peak intensity of the collimated pulse to that of the total pulse, as shown in Fig. 7. The error in measurement was smaller than shot-to-shot variation shown by the range of shots. In the earlier-reported measurements at lower energy shown in

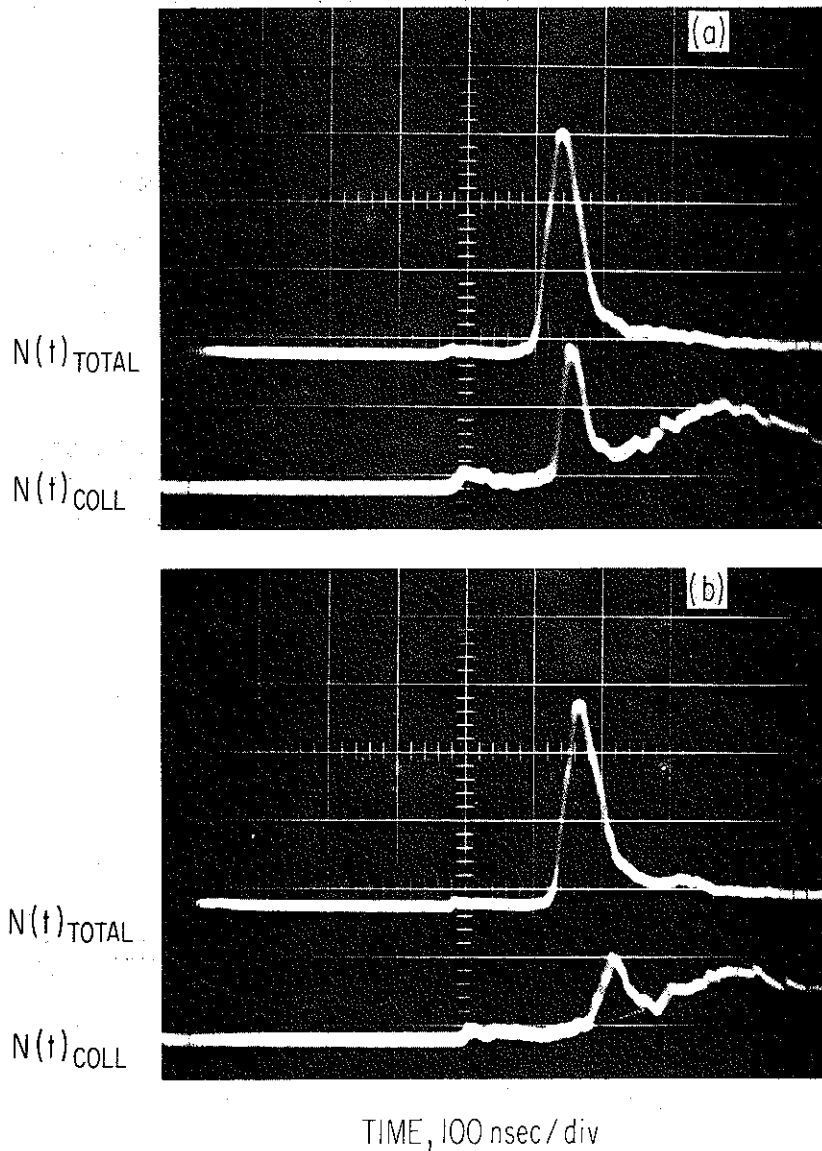


Figure 6. Neutron Collimation Measurements

(Collimated signal shows large signal because of late arrival of scattered neutrons.

Horizontal displacement of 0.2 division between traces.)

- a. Center of collimating slot 7.5 mm above anode
- b. Collimator 30 mm above anode

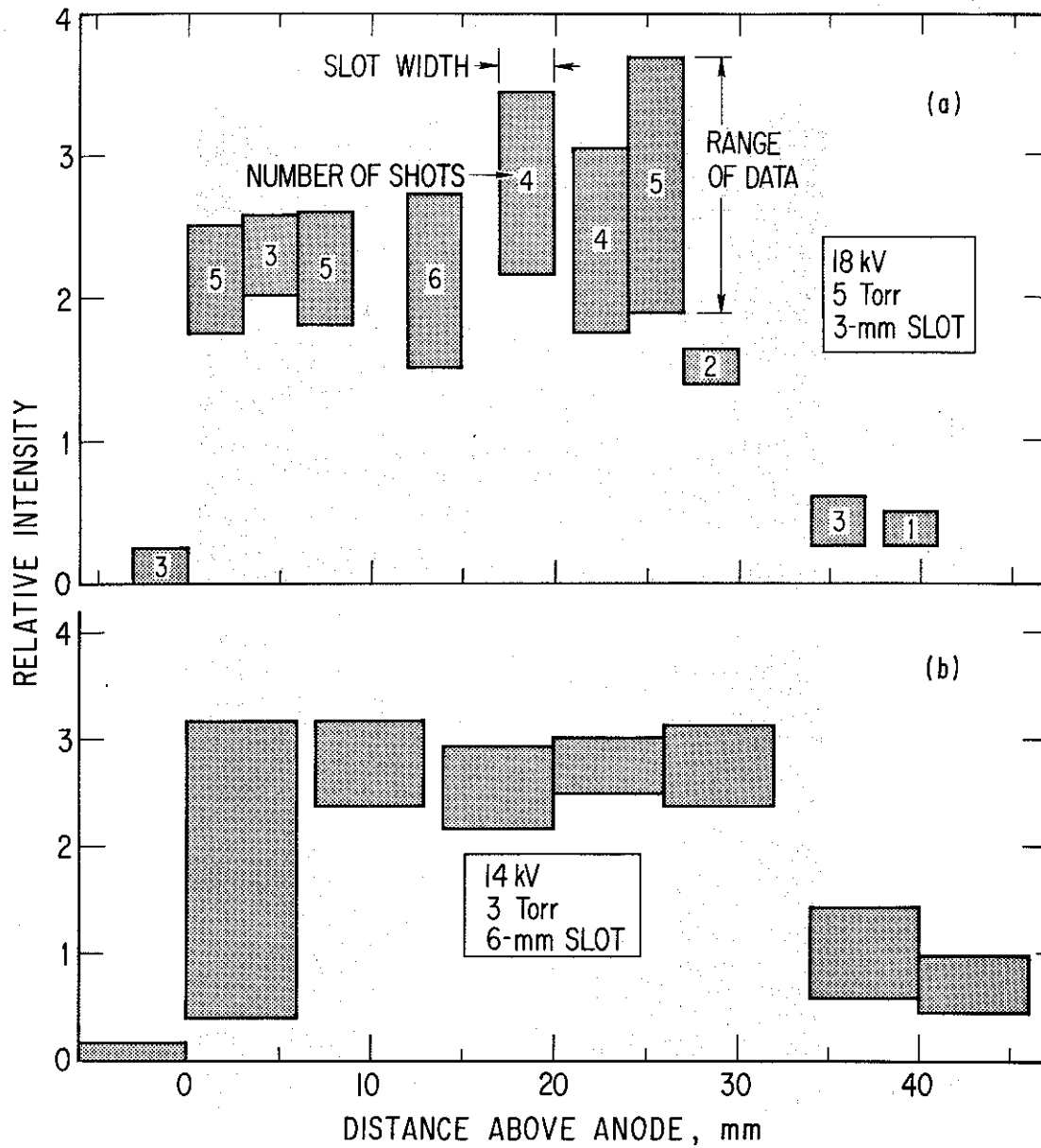


Figure 7. Axial Distribution of Neutron Intensity

(Peak intensity of collimated pulse normalized to total pulse)

- a. Operation at 18 kV with 5-Torr D_2
- b. Operation at 14 kV with 3-Torr D_2

Fig. 7b, ¹⁸ the neutron source is seen to be slightly higher above the anode tip. The average time from the beginning of the neutron production to the peak intensity of the collimated pulse was plotted as a function of axial position, as shown in Fig. 8a. Finally, the data were averaged and cross-plotted to give the time history of the intensity distribution shown in Fig. 8b for a typical neutron pulse.

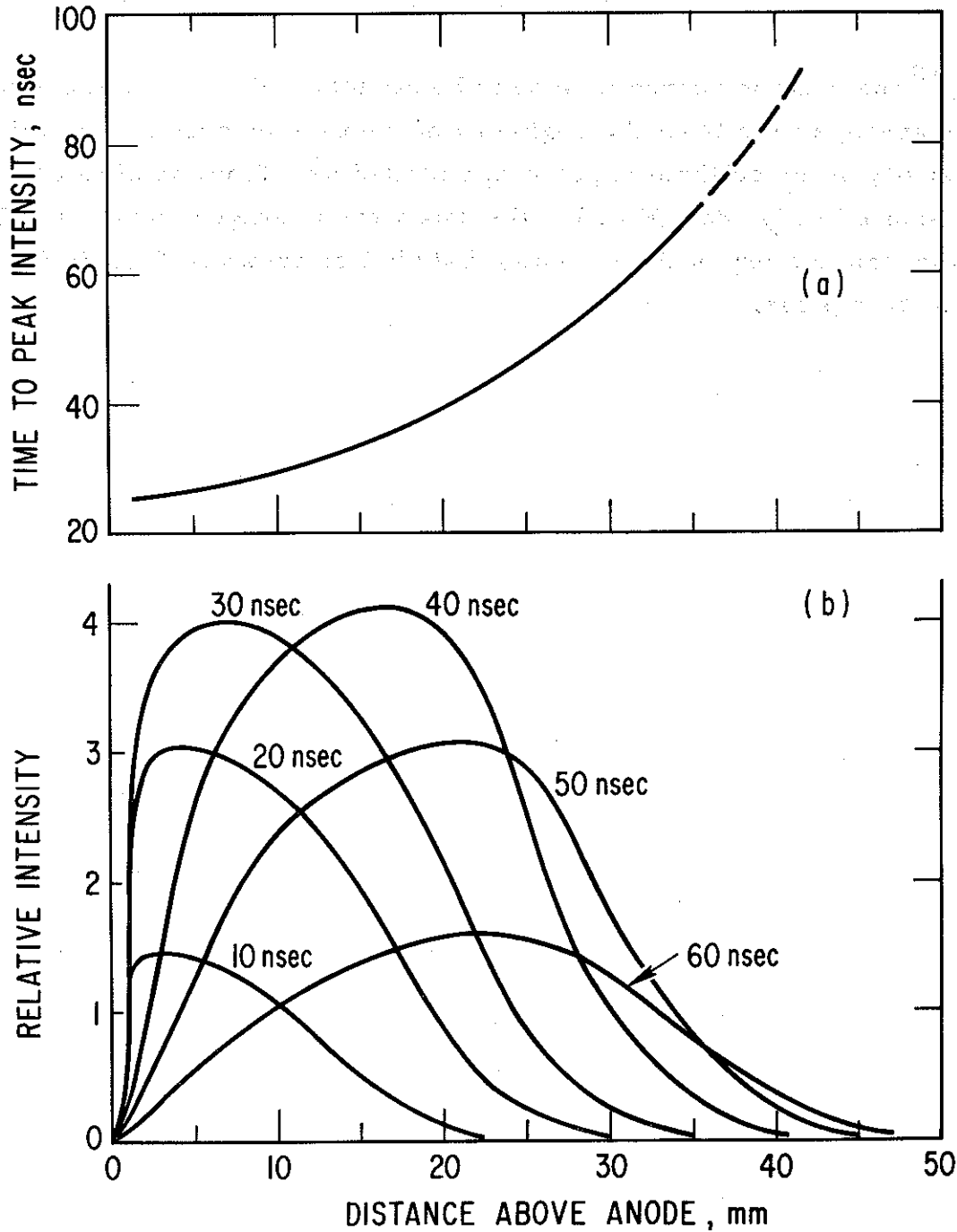


Figure 8. Time History of Neutron Source as a Function of Axial Position

- a. Average time to peak intensity of collimated pulse measured from beginning of neutron production
- b. Average intensity distribution at different times

V. ANALYSIS OF NEUTRON MEASUREMENTS

The results of our nuclear-emulsion measurements show that the neutrons emitted outward along the axis have an average energy of 3.0 MeV. Earlier nuclear-emulsion studies showed a smaller shift.¹⁹ The average energy shifts of about 450 keV obtained from our time-of-flight measurements at peak neutron intensity are in good agreement with the nuclear-emulsion studies. This is in contrast to the smaller energy shifts measured from the leading edges of the neutron pulses. Thus, for short flight paths (a few meters), the most energetic neutrons are not necessarily determined from the leading edges of pulses. The lack of 2.45-MeV neutrons in the emulsion spectra is confirmation that the neutron source has a high velocity during the entire neutron pulse.

Such neutron-energy shifts correspond to the reacting deuterons having an axial c.o.m. velocity of 2×10^8 cm/sec. As previously mentioned, this c.o.m. velocity could be explained either by an acceleration model in which directed deuterons strike stationary deuterons or by a streaming plasma model in which a hot plasma has a high axial velocity. For both models, calculations of the expected laboratory flux ratios have been made²⁰ using experimental²¹ and theoretical²² values of the D-D cross section. For a moving isotropic plasma, the flux ratio between 0 deg and 90 deg is $F(0)/F(90) = (1 + \gamma)^{3/2}/(1 - \gamma)^{1/2}$, where $\gamma = \Delta E_n/2W$ and $W = 2.45$ MeV. For an energy shift of 500 keV, an axial-acceleration model gives a flux ratio of 2.7, which is much larger than the measured ratio.

In column 3 of Table 1 calculated values are given of the expected flux ratios for moving isotropic plasmas that give the indicated shifts in neutron energy. Agreement between the calculated and measured flux ratios occurs for a ΔE_n of about 360 keV. Neutron fluxes from plasmas with a two-dimensional distribution of velocities have been considered, and calculations give an anisotropy in the radial direction of 18 to 25%.²³ The magnitude of

this anisotropy in the c.o.m. depends on both the distribution and average energy of the deuterons. Using these results, we have calculated the expected laboratory flux ratios for a two-dimensional plasma having a high axial velocity. The results for a 2-keV plasma are shown in column 4 of Table 1, and agreement between the calculated and measured values is found for a ΔE_n of about 620 keV. It appears, therefore, that the velocity distribution lies between that of a two- and three-dimensional plasma.

The high c.o.m. velocity of the deuterons obtained from the neutron-energy measurements can be correlated with other observations. From the shift in the time-dependent location of the neutron-producing region, shown in Fig. 8, an axial velocity of up to 2×10^8 cm/sec is obtained. Also framing-camera pictures show a rod-shaped region of intense luminosity forming next to the anode and then moving upward at a velocity greater than 10^8 cm/sec. Such axial velocities correspond to directed kinetic energies of up to 40 keV per deuteron.

Results of streak-photography measurements of the luminous plasma, such as shown in Fig. 2, gave maximum radial velocities of 3.2×10^7 and 4.1×10^7 cm/sec at heights of 0.8 and 1.8 cm above the anode, respectively. The lower value agrees well with one-dimensional snowplow calculations, such as have been reported for this type of pinch.²⁴ These radial velocities correspond to directed energies of 1.0 and 1.7 keV per deuteron. Three-dimensional thermalization of this kinetic energy would yield ion temperatures of only 1 keV. If a maximum plasma volume of 0.1 cm^3 (length 3 cm and radius 1 mm) is assumed and the neutron production time of 40 nsec is used, this temperature requires a density of at least $3 \times 10^{20} \text{ cm}^{-3}$ to produce yields $\sim 10^{10}$. Complete pinching of all gas above the anode would produce a density of $4 \text{ to } 5 \times 10^{20} \text{ cm}^{-3}$. A two-dimensional Maxwellian distribution would have a higher temperature, but for a density of 2×10^{20} and a temperature of 2 keV, the ion thermalization time is less than 1 nsec.²⁵ Directed kinetic energy of the collapsing ions is not the sole criterion for producing high neutron yields, since operation at lower pressures gives

slightly higher radial velocities but no increase in neutron yield. The rapid thermalization time does not agree with the nonisotropic plasma inferred from the neutron measurements.

It appears that uniform plasma parameters inferred from visible-light observations are insufficient to account for the observed neutron production. Therefore, we consider other processes in the plasma. The megagauss magnetic fields, which are produced by contraction of the discharge current to radii less than 1 mm, create ultrahigh radial pressures in the plasma. Then, because of the nonsimultaneous pinching of the curved plasma sheath, very large axial pressure gradients are set up. In order to estimate the rate of plasma expansion, we have made one-dimensional calculations similar to three-dimensional calculations for a laser-produced plasma.²⁶ A cylinder of plasma that expands axially is assumed and the work done in plasma expansion is equated to the increase in kinetic energy.

$$-\int_0^L \frac{\partial P}{\partial z} \frac{\partial z}{\partial t} dz = \frac{1}{2} \frac{d}{dt} \int_0^L n_i m_i \left(\frac{dz}{dt} \right)^2 dz$$

where P is the plasma pressure, m_i is the ion mass, n_i is the ion density, and L is the length of the expanding plasma. A spatially uniform temperature is assumed, and the density and pressure are allowed to decrease linearly across the length of the expanding plasma. If it is further assumed that the density profile stays constant, the axial velocity increases linearly along the length of the plasma. Using the maximum plasma pressure and letting the plasma start from rest, we obtain an expansion velocity

$$v \approx 12kT\Delta t/m_i L$$

where T is the plasma temperature, and Δt is the time the plasma has been expanding. For gradients across a few millimeters and times of a few

nanoseconds, expansion velocities of about 6×10^7 cm/sec are found for a plasma starting from rest, but this streaming velocity will be greatly increased as follows. The confining magnetic field will compress the remaining plasma to higher temperatures increasing the expansion velocity, and the streaming plasma will be compressed by the pinching action further up the axis, which also adds to the axial velocity. Therefore, we conclude that, because of axial ejection of plasma after the initial collapse, the magnetic field compresses the remaining plasma to temperatures somewhat higher than that assumed from the collapse velocity.

VI. X-RAY MEASUREMENTS

A. EXPERIMENT

Spectra of the x rays emitted by the discharge in the energy range of 7 to 29 keV were measured with a set of Ross filters.²⁷ A Ross filter consists of two thin foils matched in thickness so that the difference in transmitted flux gives the x-ray energy in the interval between the two K edges of the elements (Kodak Type F x-ray film was used as a detector). Experimental details will be given in a future paper. The filters were placed on axis and viewed the discharge end-on through a beryllium window. Small variations in flux intensity over the area of the filter set were accounted for in the analysis. Also taken into account was the attenuation due to the window and the air. The major errors occurred in reading the film densities and subsequently taking the difference of two readings.

Spectra were measured using anodes of copper and copper with tungsten or silver inserts (insert diameter was 20 mm). Representative examples of the measured spectra are given in Fig. 9. No correlation was found between the spectra and neutron yield. All spectra showed a continuum plus strong line emission by the $K\alpha$ and $K\beta$ fluorescence lines of copper at 8.0 and 8.9 keV. In addition, the fluorescence lines of silver appeared when the silver insert was used. Time-resolved x-ray measurements made using two matched silicon detectors with two Ross-filter foils showed that the shape of the continuum spectra did not change with time.

Side-on pinhole photographs of the discharge were made through beryllium windows having thicknesses of 3.2 and 0.05 mm. An example is shown in Fig. 10. The filtering effect of the thicker window was used to estimate the flux in the energy range below 7 keV down to 2 or 3 keV. Assuming flux isotropy, this low-energy radiation was estimated to be on the

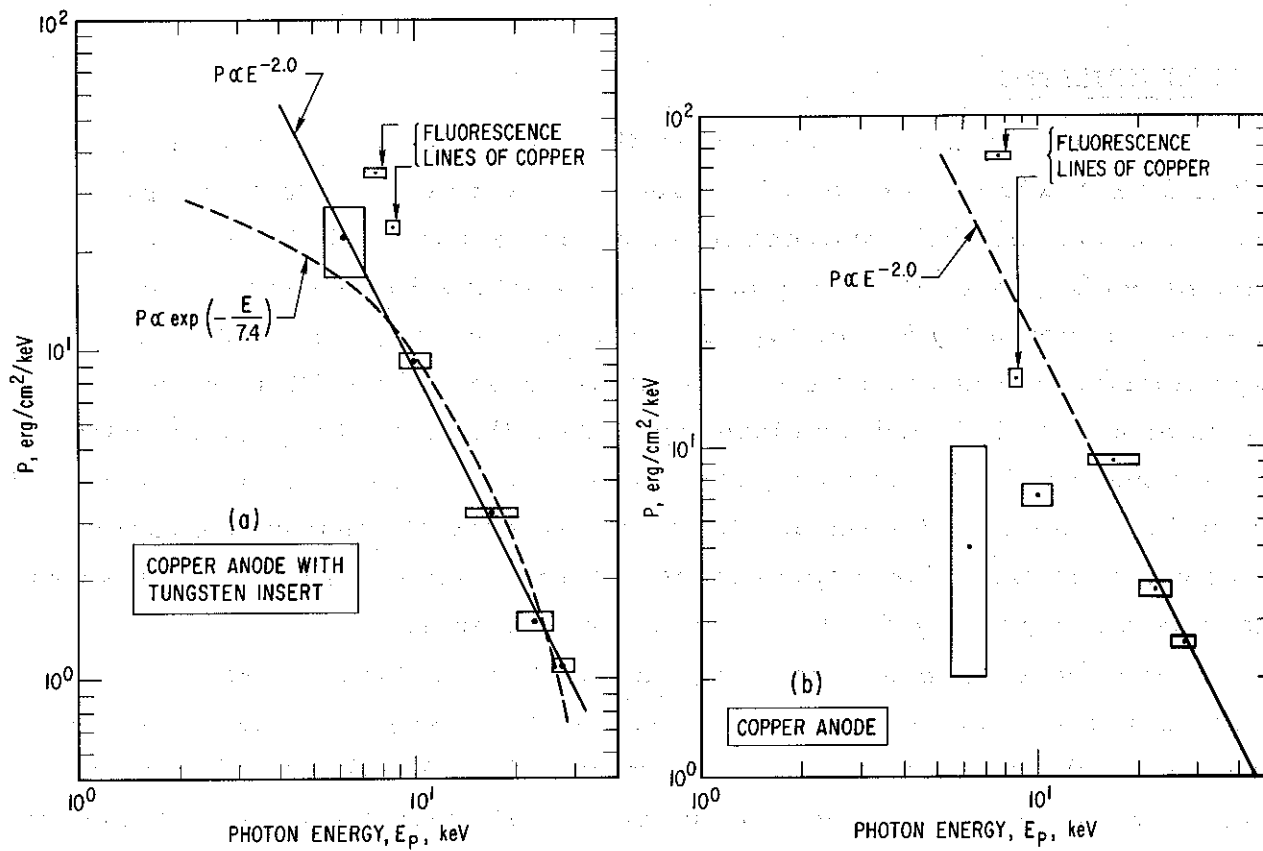


Figure 9. X-Ray Spectra With Ross Filters
 [Operation at 14 kV (17 kJ)]



25mm

78 mm
ANODE DIAM

Figure 10. Side-on X-Ray Pinhole Photograph
Through 0.05-mm-thick Be Window

order of 10 J for a bank energy of 17 kJ, whereas the radiated energy in the range of the Ross filters was about 0.3 J.

B. INTERPRETATION OF X-RAY RESULTS

On all shots with the tungsten insert, the continuum can be represented very well by an $E_p^{-(2.10 \pm 0.10)}$ power-law dependence, where E_p is the photon energy. An E_p^{-2} dependence was also found for the continuum when using a silver insert. On the other hand, use of an all-copper anode gave a continuum with a broad peak at about 15 keV. This is interpreted as filtering of an E_p^{-2} spectrum through a few mg/cm^2 of anode material. In fact, measurements of the anode erosion show that the average amount of copper lost on each shot is two orders of magnitude greater than that needed to produce the filtering effect.

With a copper anode, the intensity ratio of the $K\alpha$ to $K\beta$ fluorescence lines (measured above the continuum) was about 6 to 1. This corresponds to the line radiation of cold copper.²⁸ The intensity ratio of the copper lines obtained with a tungsten insert corresponded to multiply-ionized copper, but the degree of ionization was not determined. In any case, the copper ions were not hydrogen-like, since all the line emission was not in the higher energy interval. It is noteworthy that a significant number of copper ions were found in the discharge when inserts of other metals were on axis.

As shown in Fig. 9a, the Ross-filter data could marginally be fit with a Bremsstrahlung curve assuming a temperature of 7.4 keV. However, the 10 J of energy found in the range below 7 keV exceeds by an order of magnitude the amount of energy estimated by extrapolating the E_p^{-2} spectral curve down to about 2.5 keV. This magnitude of low-energy radiation can be accounted for by Bremsstrahlung from a contaminated high-density plasma when assuming the same plasma parameters used to estimate the neutron production.

In order to explain the E_p^{-2} power law of the measured spectra, processes other than a thermal plasma must be considered. It appears that

the high-energy x radiation arises from the acceleration of electrons into high-z ions. However, the usual x-ray tube type of spectrum is unsatisfactory in explaining the spectra. It is well known that x-ray tubes operated at voltages below 100 kV produce spectra in which the x-ray intensity rises from zero at $E_p = V$ to a maximum at $E_p = 2V/3$ and then falls off at lower energies. It is possible to formulate a distribution of electron current as a function of electron energy that would give the observed spectra. However, for electrons of these energies, there is negligible x radiation in the backward direction, because the forward-directed Bremsstrahlung produced by the impinging electrons is absorbed much more readily than scattered.

On the other hand, x radiation with energies over 300 keV has been detected. Photons in the energy range over 100 keV will be scattered many times before they lose all their energy. Therefore, we believe that the observed x-ray spectra arise from accelerated electrons creating high-energy Bremsstrahlung, which is then scattered and reradiated at lower energies.

VII. CONCLUSIONS

The stored magnetic energy in a coaxial-electrode device drives a rapid radial collapse of the plasma across the end surface of the center anode. Contraction of the discharge current to a radius of a millimeter or less creates very high magnetic-field pressures, which compress the plasma to an initial density of a few times 10^{20} cm^{-3} . Since the pinching action is not simultaneous along the axis, very high pressure gradients are set up. This causes a rapid expansion of plasma along the axis, and velocities of $2 \times 10^8 \text{ cm/sec}$ are attained. Plasma temperatures of 1 to 2 keV and densities of $2 \times 10^{20} \text{ cm}^{-3}$ are sufficient to explain the neutron production, but the neutron energy and flux measurements indicate an anisotropic plasma. A better understanding of the processes in the dense pinch requires knowledge of the plasma density, temperature, and current density with a resolution much better than a millimeter.

There is some question as to what limits the lifetime of the neutron production. The three possibilities to be considered are radiation cooling, instability breakup of the plasma, and a large decrease in the plasma density due to axial streaming. On the time scales involved here, the radiation losses do not appear large, even with significant amounts of impurity ions in the plasma. Calculations have shown that the $m = 0$ growth rate is slowed considerably by the curved nature of the pinch and its short length.²⁹ But the calculated instability growth times are still comparable to the observed production times. A decrease in plasma density can, of course, increase the growth rate of the instabilities. If the neutron production is limited only by the axial losses of plasma, then axial injection of plasma may bring a considerable enhancement. It may be that axial streaming is a necessary condition for high neutron yields.

The observed x-ray spectra arise most likely from the anode bombardment of electrons in the energy range greater than 200 keV. Most of the

high-energy photons are scattered and reradiated at lower energies. No calculations or measurements are known that determine the shape of the x-ray spectra well below 100 keV from the anode bombardment of these high-energy electrons.

REFERENCES AND FOOTNOTES

1. N. V. Filippov, T. I. Filippova, and V. P. Vinogradov, Nucl. Fusion Suppl., Pt. 2, 577 (1962).
2. J. W. Mather, Phys. Fluids 8, 366 (1965).
3. E. H. Beckner, J. Appl. Phys. 37, 4944 (1966).
4. D. A. Meskan, H. L. L. van Paassen, and G. G. Comisar, Proceedings of the LASL Topical Conference on Pulsed High Density Plasmas, LA-3770 (September 1967).
5. J. W. Mather, Plasma Physics and Controlled Nuclear Fusion Research (International Atomic Energy Agency, Vienna, 1966), Vol. II, p. 389.
6. N. V. Filippov and T. I. Filippova, *ibid*, p. 405.
7. J. W. Mather, et al., Bull Am. Phys. Soc. 13, 1542 (1968).
8. T. F. Stratton, Plasma Diagnostic Techniques, ed. R. H. Huddlestone and S. L. Leonard (Academic Press, 1965).
9. J. W. Mather and A. H. Williams, Rev. Sci. Instr. 3, 297 (1960).
10. J. W. Mather and P. J. Bottoms, Phys. Fluids 11, 611 (1968).
11. W. Barkas, Nuclear Research Emulsions (Academic Press, New York, 1963).
12. R. Stephen White, "Photographic Plate Detection," in Fast Neutron Physics, Vol. 1, ed. J. B. Marion and J. L. Fowler (Interscience Publishers, Inc., N. Y., 1960).
13. D. A. Meskan, H. L. L. van Paassen, and G. G. Comisar, "Neutron and X-Ray Production in a Focused Z-Pinch," Aerospace Corp. Report No. TR-0158(3220-50)-1 (December 1967).
14. Similar measurements without collimators showed the anisotropy was reduced by about 5%. In addition, measurements of the flux with time-integrated Ag-counters gave a flux ratio of 1.11 ± 0.04 , but neither room scattering nor the energy dependence of the counters was taken into account.

15. M. Gettner and W. Selove, *Rev. Sci. Instr.* 31, 450 (1960)
16. R. Honecker and H. Grässler, *Nucl. Instr. and Methods* 46, 282 (1967).
17. J. L. Gammel, Fast Neutron Physics, Part II, ed. J. B. Marion and J. L. Fowler (Interscience Publishers, Inc. N.Y., 1960).
18. M. J. Bernstein, *Bull. Am. Phys. Soc.* 13, 879 (1968).
19. A. M. Andrianov et al., Proceedings Second U.N. Conf. on Peaceful Uses of Atomic Energy, 31, 348 (1958).
20. G. G. Comisar, Private Communication, Aerospace Corp.
21. D. L. Booth, G. Preston, and P. R. Shaw, *Proc. Phys. Soc. (London)* 69A, 265 (1956).
22. E. J. Konopinski and E. Teller, *Phys. Rev.* 73, 822 (1948).
23. G. Lehner and F. Pohl, *Zeit. f. Physik* 207, 83 (1967).
24. C. Patou, A. Simonnet, and J. P. Watteau, *Proc. of the LASL Topical Conference on Pulsed High Density Plasmas*, LA-3770 (September 1967).
25. L. Spitzer, Jr., Physics of Fully Ionized Gases (Interscience Publishers, Inc., N. Y., 1962).
26. A. F. Haught and D. H. Polk, *Phys. Fluids* 9, 2047 (1966).
27. P. A. Ross, *J.O.S.A.* and *R.S.I.* 16, 433 (1928).
28. H. A. Liebhafsky et al., X-Ray Absorption and Emission in Analytical Chemistry (John Wiley & Sons, N.Y., 1960).
29. G. G. Comisar, *Phys. Fluids*, to be published.